Journal of Applied Physics

Bond length fluctuation in perovskite chromate $SrCrO_3$

Cite as: J. Appl. Phys. **127**, 075106 (2020); https://doi.org/10.1063/1.5131406
Submitted: 12 October 2019 . Accepted: 18 January 2020 . Published Online: 19 February 2020

Yifan Ding, Lipeng Cao, Weipeng Wang, Boyu Jing, Xi Shen, Yuan Yao, Lifang Xu, Junjie Li, Changqing Jin, and Richeng Yu

AIP Publishing

Journal of Applied Physics ARTICLE scitation.org/journal/jap

Bond length fluctuation in perovskite chromate $SrCrO_3$

Cite as: J. Appl. Phys. **127**, 075106 (2020); doi: 10.1063/1.5131406
Submitted: 12 October 2019 · Accepted: 18 January 2020 ·
Published Online: 19 February 2020

Yifan Ding,[1,2] Lipeng Cao,[1] Weipeng Wang,[1,2] Boyu Jing,[3] Xi Shen,[1] Yuan Yao,[1] Lifang Xu,[1] Junjie Li,[1] Changqing Jin,[1,2] and Richeng Yu[1,2,a)]

AFFILIATIONS

[1]Beijing National Laboratory of Condensed Matter Physics, Institute of Physics, Chinese Academy of Sciences, Beijing 100190, People's Republic of China
[2]School of Physics Sciences, University of Chinese Academy of Sciences, Beijing 100049, People's Republic of China
[3]Class of 2018 AP Program, International Department of Beijing National Day School, Beijing 100039, People's Republic of China

[a)]**Author to whom correspondence should be addressed:** rcyu@iphy.ac.cn

ABSTRACT

Perovskite chromate $SrCrO_3$ containing Cr^{4+} ions shows anomalous electronic states and physical properties, which are believed to be related to the bonding instability, but this has not been confirmed directly in experiments up to now. In order to address this issue, the crystal structure and electronic structure of $SrCrO_3$ are investigated by using transmission electron microscopy and first-principles calculations. The results demonstrate that there is no fourfold rotational symmetry in the selected area electron diffraction patterns along the three main zone axes of $SrCrO_3$, which is inconsistent with an expected cubic structure. Moreover, the orientation-dependent electron energy-loss spectra demonstrate a clear correlation between the dissimilar spectra and the anisotropic effects derived from the crystal structure, and first-principles calculations support the experimental results. All this strongly supports the bonding instability of ambient pressure and temperature phase of $SrCrO_3$ and highlights the important influence of bonding fluctuation on its electronic structure and transport properties. The influence of the core-hole effect and Hubbard potential on the theoretical spectra is further investigated.

I. INTRODUCTION

Perovskite and perovskite-like compounds are important, especially in oxide functional materials. A large number of functional materials, including piezoelectrics,[1] ferroelectrics,[2] and magnetoresistance,[3] belong to this category and have been used in many areas. Because of the competition among charge, spin, orbit, and lattice, these materials manifest abundant physical properties. Perovskite chromate $ACrO_3$ (A = Ca, Pb, Sr) containing unusual high-oxidation state Cr^{4+} with two electrons in Cr 3d shell is particularly intriguing on account of anomalous electronic states and physical properties, and its orbital angular momentum is not fully quenched. Since its radius is too small to form sixfold octahedral coordination stably, the Cr^{4+} ion preferentially forms fourfold tetrahedral coordination,[4] and, therefore, the perovskite chromate containing Cr^{4+} ions needs to be prepared under high temperature and high pressure. Though perovskite chromates $ACrO_3$ (A = Ca, Pb, Sr) were first synthesized in the late 1960s, the detail of neither the crystal structure nor the anomalous physical properties is still not very clear. Generally, an insulator coexists with antiferromagnetism, while metallic conductivity coexists with ferromagnetism. However, $CaCrO_3$, an orthorhombic perovskite chromate, is a rare antiferromagnetic metal with a peculiar electronic state,[5,6] lying in the intermediate regime between the Mott–Hubbard system and the charge-transfer system. The $PbCrO_3$ possesses a cubic perovskite but with an abnormally large volume, and it was reported that $PbCrO_3$ has a volume collapse in an iso-structural transition at around 1.6 GPa,[7] and a complex modulated superstructure appears because of Pb deficiency,[8] which has been rarely studied probably due to the same difficulty in synthesizing it as in preparing $SrCrO_3$, and the reported experimental results about electronic and magnetic properties of the $PbCrO_3$ are still controversial. Chamberland *et al.* first reported that $SrCrO_3$ is of a cubic perovskite structure with Pauli paramagnetic metal state,[9] and its resistivity measured by Williams *et al.*[10] manifests also metallic behaviors. In contrast, Zhou *et al.*[11] proposed that the polycrystalline $SrCrO_3$ is in a

nonmagnetic insulating state at ambient pressure, but turns into a metallic state as pressure increases. Williams *et al.*[10] found a sharp peak in the curve of $SrCrO_3$ magnetization vs temperature, indicating that there is a magnetic transition at 50 K, which is consistent with the result of Ortega-San-Martin *et al.*[12] However, there is no sharp peak in the magnetic susceptibility measured by Zhou *et al.*[11] and Alario-Franco *et al.*[13] Zhou *et al.*[11] believed that the perovskite chromate containing Cr^{4+} and CrO_6 octahedron is located close to the crossover between metal and insulator, resulting in an anomalous electronic structure and novel physical properties. In addition, powder neutron diffraction results at different temperatures, reported by Williams *et al.*,[10] suggested that $SrCrO_3$ has a cubic structure at 100 K and its (311) peak splits at 10 K, indicating a structural transition in a temperature range of 10–100 K. These results are in agreement with the results of Ortega-San-Martin *et al.*[12] that a tetragonal phase and a cubic phase coexist at low temperature, and a tetragonal phase with C-type antiferromagnetic structure appears below 40 K, accompanied by orbital ordering. Alario-Franco *et al.* reported that the Cr ion is in an unusual +4 oxidation state by electron energy-loss spectrum.[14] With first-principles calculations, Lee and Pickett[15] reported that a slightly tetragonally distorted structure is more stable in terms of energy, which accords with the experimental result of Ortega-San-Martin *et al.*[12] Furthermore, Lee and Pickett[15] proposed that the tetragonal phase undergoes an orbital-ordering transition when U is larger than 4.0 eV. However, Qian *et al.*[16] reported that $SrCrO_3$ is an antiferromagnetic metal with relatively weak correlation strength ($U < 3.0$ eV). Though these are in conflict with experimental results for high-pressure synthesized $SrCrO_3$, its potential applications can be identified. The $(SrCrO_3)_1/(SrTiO_3)_1(001)$ superlattice possessing large room-temperature Seeback coefficients exhibits excellent thermoelectric properties.[17] In addition, the perovskite $SrCrO_3$ and rhombohedral $SrCrO_{2.8}$ can be transformed into each other under artificially controlled experimental conditions, and the latter can be used as a solid oxide fuel cell due to its active oxygen ion conductivity.[18]

As is well known, x-ray diffraction (XRD) provides information about the average structure, and previous x-ray diffraction studies did not present any detail of bond length difference of $SrCrO_3$ and showed that it possesses a cubic structure.[9,10] Aberration-corrected transmission electron microscopy (TEM) and electron energy-loss spectroscopy (EELS) provide a powerful approach to investigating the structural distortion and the electronic structure, respectively, and density functional theory calculations conduce to the understanding of EELS. The high spatial resolution opens up possibilities for studying the atomic-scale bonding and the electronic structure, which is beneficial to better understanding the properties of materials. Annular bright-field (ABF) image in scanning transmission electron microscopy (STEM) mode has the advantage of detecting light elements, while high-angle annular dark-field (HAADF) image possesses the merit that small change in specimen thickness and defocusing have little influence on the image contrast. Although lattice distortions can be investigated by using imaging techniques, spectroscopic techniques will provide additional unique information about the structural and chemical environment of each ion. When an electron in the inner shell is excited to a high-level unoccupied state, a core hole will remain in the inner shell, which will change the local electron potential field and thus affecting the electron density of the system. The O 1s spectrum is successfully used as a probe for studying the distortion of $BaTiO_3$ because lattice distortion leads to the anisotropic effects of core-hole potential.[19] In our experiments, we choose O 1s spectrum to investigate the lattice distortion of $SrCrO_3$, which proves to be very effective in detecting the detail of the local electronic structure.

In view of the fact that the results about $SrCrO_3$ are still controversial, we investigate them carefully by aberration-corrected TEM and orientation-dependent EELS in this work. The TEM images suggest that $SrCrO_3$ does not possess cubic symmetry. The near-edge fine structure of the O-K edge of $SrCrO_3$ is highly sensitive to chemical bonds, and the slight change of the Cr–O bond length will affect the electrons locating in different orbitals, which is indicated in the orientation-dependent EELS. Here, we show that $SrCrO_3$ is not of a cubic structure, for Cr–O bonds in three main zone axes are not strictly equal in length, which indicates the bond length fluctuation instability.

II. METHODS

Single crystal $SrCrO_3$ was prepared by solid-state reaction method under pressure. After being fully mixed in a glove box filled with argon, the starting materials SrO and CrO_2 were pressed into pellets and then sealed into gold capsules. The $SrCrO_3$ compound was synthesized at 5.5 GPa and 1000 °C for 30 min. The single crystal sample was checked by single crystal x-ray diffraction (XRD) and powder XRD, separately. The detailed preparation of the samples was described in Ref. 20. The specimens for TEM were prepared by using a focused ion beam (FIB), and the amorphous layer on its surface was cleaned by a very weak Ga ion beam.

Aberration-corrected STEM, selected area electron diffraction (SAED), and orientation-dependent EELS were performed on a JEOL ARM200F aberration-corrected TEM equipped with a Gatan GIF Quantum ER spectrometer. Its available spatial resolution of STEM images is better than 78 pm at 200 kV. In this work, the diffraction mode (image coupling) was used to obtain the orientation-dependent EELS.

Theoretical calculations for the O-K orientation-dependent near-edge fine structure were implemented with the WIEN2k package,[21] which is based on the full-potential linearized augmented plane-wave method. The generalized gradient approximation (GGA) of Perdew, Burke, and Ernzerhof[22] exchange-correlation functional was applied to the energy-loss near-edge structure (ELNES) simulation. The muffin-tin radius was set to be 2.40, 1.78, and 1.61 bohr for Sr, Cr, and O, respectively. The core hole left by the excited electron was implemented in the simulations through using a $2 \times 2 \times 2$ supercell, which was created to minimize the interactions between neighbor core holes, and the missing electron was added to the background charge to ensure the crystal neutrality. The plane-wave cutoff, RK_{max}, was set to be 7.0. Self-consistency cycle convergence was achieved with 80 and 725 k points in the irreducible wedge of the Brillouin zone and whole Brillouin zone, respectively. An effective Hubbard potential $U_{eff} = U - J = 2.9$ eV ($J = 0$ eV) was used to correct the Cr 3d state energy.

III. RESULTS AND DISCUSSION

The ABF image, HAADF image, and SAED pattern along the [100] zone axis are shown in Figs. 1(a)–1(c), respectively, and they look like they have a cubic symmetry as reported previously.[9,10] However, the SAED patterns indicate that $SrCrO_3$ does not possess a cubic symmetry. Figure 1(d) shows the operation process, i.e., rotating the original SAED pattern in the upper left corner 90° (see the resulting figure in the lower left corner), and the green arrow indicates that the rotated SAED pattern overlaps with the original pattern. If the sample is of a cubic structure, the two SAED patterns should coincide with each other. Our results are shown in Fig. 1(e), and the spots can be seen to be misaligned at a distance from the central spot. Two other sheet-like samples along the [010] and [001] zone axes are also prepared from the same single crystal for TEM experiments by using an FIB technique. Figures 1(f) and 1(g) along the [010] and [001] zone axes also show misaligned spots far from the central spot, and Fig. 1(h) enlarges the misaligned positions of Fig. 1(g) for the illustrative purpose.

In order to further investigate the crystal symmetry of $SrCrO_3$, the orientation-dependent EELS is utilized to investigate the minor change in crystal symmetry. For an anisotropic material, the magnitude and orientation of momentum transfer can be detected by changing the relative orientation between the incident electron beam and the crystal.[23] Therefore, the electronic structure and asymmetry of the crystal structure can be investigated by orientation-dependent EELS. In this study, the orientation-dependent EELS spectra are recorded in the diffraction mode (image coupling) with the spectrometer aperture centered on the direct beam. The 0.37 mrad convergence angle and the 0.75 mrad collection angle are small enough to detect the momentum transfer parallel to the electron beam. Therefore, the momentum transfer parallel to the incident beam is dominant. In order to understand the orientation-dependent EELS, it is necessary to construct a crystal structure model and calculate the electronic structure.

Figure 2(a) shows the schematic representation of the crystallographic structure of the orthorhombic $SrCrO_3$ structure by VESTA software. When the electron beam is parallel to the *a* axis, the peak in the O-K edge mainly comes from the transition from the O 1s state to the unoccupied O p_x state. It is similar to the scenario when the electron beam is parallel to the other two directions, separately. Experimental orientation-dependent O-K EELS spectra shown in Fig. 2(b) (solid lines) exhibit different features, indicating different symmetries along the three main zone axes.

Based on the above-mentioned experimental results, an orthorhombic structure $SrCrO_3$ with Pmmm space group shown in Fig. 2(a) is constructed and optimized by using Wien2k. The optimized unit cell parameters for the orthorhombic $SrCrO_3$ are $a = 3.7925$ Å, $b = 3.8448$ Å, and $c = 3.7536$ Å; the atomic positions of Sr, Cr, and O are (0,0,0), (0.5,0.5,0.5), and (0.5,0,0.5), respectively. It should be noted that according to the group theory, Pmmm is a subgroup of Pm-3m. The structure is shown in Fig. 2(a), and its simulated electron diffraction patterns (shown in Fig. S1 in the supplementary material) are consistent with the measured ones. Figure 2(b) shows the simulated orientation-dependent EELS spectra (dashed-dotted lines) of the orthorhombic structure $SrCrO_3$, which reproduces all the spectral features. The ELNES originates from the electron transition from the core shell to the unoccupied state, which is allowed by dipole selection rule, and, thus, the projected density of states (DOS) above the Fermi level can be used to explain the ELNES peaks. The calculated total and projected DOSs for Sr, Cr, and O ions are shown in Fig. 3. The first peak A of the O-K edge comes from the hybridization between the Cr 3d orbit and the O 2p orbit, and the second peak B originates from the hybridization between Sr and O 2p, while the third peak C arises from the hybridization among Sr, Cr, and O 2p. The calculated DOSs of the cubic structure are shown in Fig. S2 in the supplementary material for comparison.

There are several factors influencing EELS simulations, which need to be clarified. As shown in Fig. 2(b), the energy range for the calculated EELS spectrum is smaller than that for the measured one, and the relative intensity of the first peak of the calculated EELS spectrum is higher. A similar effect was reported by Gao *et al.*[25,26] in the calculation of the 1s core-level spectra of the second period elements. The positive core-hole potential pulls down the states in

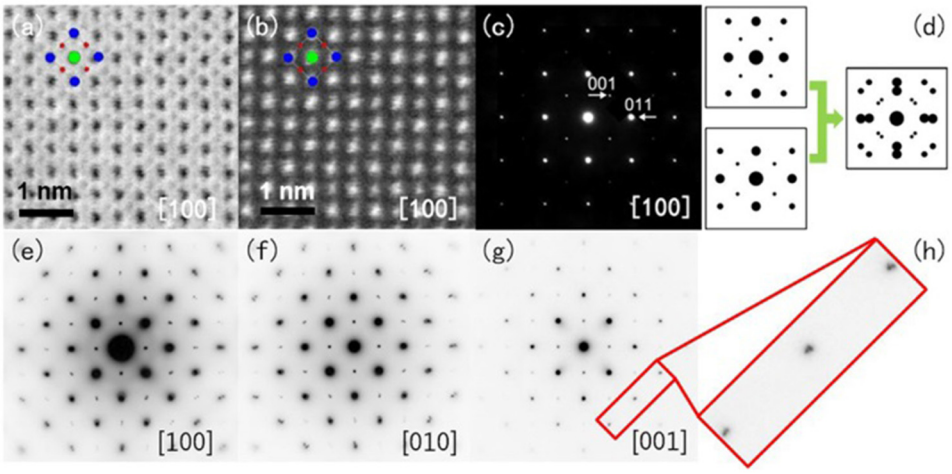

FIG. 1. STEM images and SAED patterns of $SrCrO_3$. (a) ABF image, (b) HAADF image, (c) SAED pattern {crystal model projection in panels [(a) and (b)], and indexed spots in panel (c) are based on cubic structure}. (d) Diagrammatic sketch showing a method to judge fourfold rotational symmetry, (e)–(g) contrast inverted diffraction patterns recorded along the [100], [010], and [001] zone axis, respectively, and (h) local enlargement of panel (g).

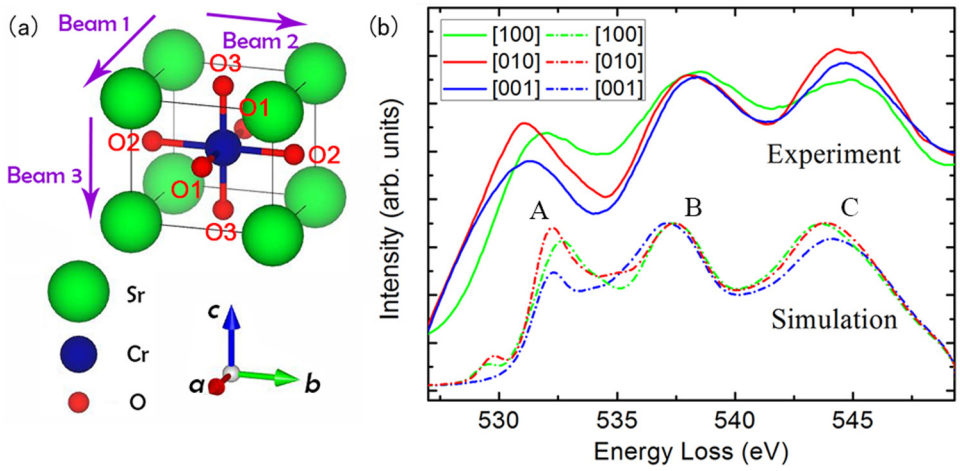

FIG. 2. (a) Schematic representation of the crystallographic structure of the orthorhombic $SrCrO_3$ structure by VESTA software,[24] where the structure is exaggerated for illustrative purpose; green ball denotes Sr, blue one Cr, and red one O (three types of O atoms are denoted as O1, O2, and O3), and each ball size is proportional to atom radius; purple arrow indicates the direction of incident electron beam. Beams 1, 2, and 3 represent electron beams incident in directions parallel to *a*, *b*, and *c* axis, respectively. (b) Experimental orientation-dependent O-K edge EELS of $SrCrO_3$, obtained with convergence angle of 0.37 mrad and collection angle of 0.75 mrad along [100] (green solid line), [010] (red solid line), [001] (blue solid line) direction; simulated orientation-dependent O-K near-edge spectra obtained under the conditions consistent with the measured ones. Simulated spectra are aligned with the peak A of measured spectra.

the conduction band toward the threshold energy and the wave function shrinks, and, thus, the spectral weight near the threshold is enhanced. Simultaneously, the influence of U_{eff} is essential. In the theoretical calculation of EELS, the correlation effect is usually taken into account in the understanding of the experimental results.[19] The Hubbard term shifts the Cr 3d energy band and further modifies O 2p states, thereby changing the intensity and position of O-K edge. The effective Hubbard potential 2.9 eV is used to correct the Cr 3d state energy, which is consistent with the value reported by Qian *et al.*[16] (Figs. S3 and S4 in the supplementary material show that changing U_{eff} does affect the peak position of the O 2p DOS and the peak position of O-K edge spectrum). In the orientation-

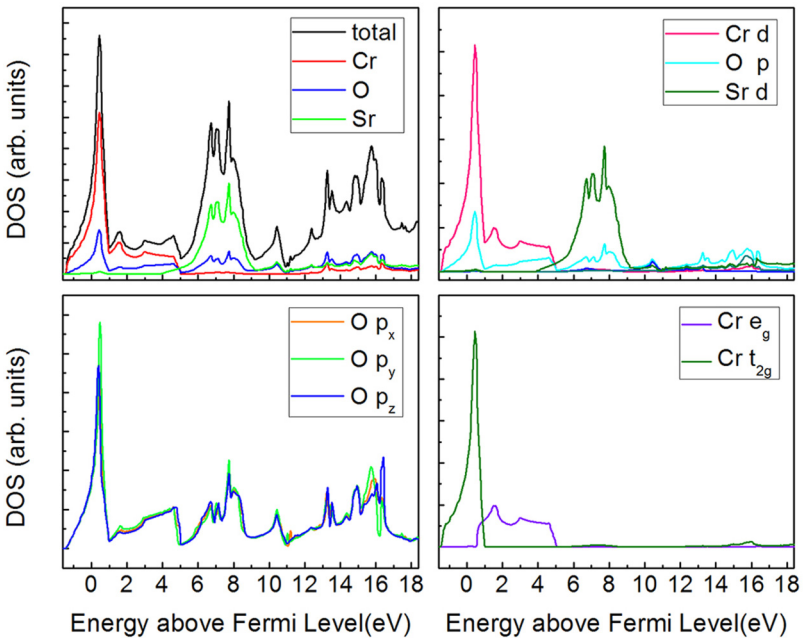

FIG. 3. Calculated total and projected DOSs for Sr ion, Cr ion, and three types of O ions.

dependent EELS simulation, the core hole is set for each of unequal O1, O2, and O3, and their spectra along the *a*, *b*, and *c* axis are calculated, respectively. The ELNES is a linear combination of unequal O atoms. When electron beam is parallel to the *a* axis, the final simulated spectrum is calculated from weighted average of the individual spectra, which means that the simulated spectra of the O1, O2, and O3 along the *a* axis are averaged at the ratio of the number of O atoms in three unequal sites, 1:1:1, to obtain the final simulated spectrum along the *a* axis. The same method is used to simulate the final spectra along the *b* and *c* axis. The individual O spectra in all three directions are shown in Fig. S5 in the supplementary material. When the Cr–O bond length changes, the structural and chemical environments around the O atom both become more complicated, and the orbital energy level also changes. These changes are directly indicated from the ELNES. It should be noted that if core holes are not taken into account, the calculated EELS spectra along the three directions have little difference from each other. Thus, the core-hole potential is an important factor in studying the EELS spectra of anisotropic materials.

Zhou *et al.*[11] reported that the bond instability can cause the bond length to fluctuate significantly and inhibit phonon thermal conductivity, leading to abnormal transport and magnetism, which are manifested in a series of anomalous properties. If the $SrCrO_3$ possesses a highly symmetric cubic structure as reported previously,[9,10] then two electrons will occupy the degenerate t_{2g} orbitals. Based on the Jahn–Teller theorem, it can cause the octahedron to be distorted, thus reducing the structural symmetry and removing the orbital degeneracy.[27] The CrO_6 regular octahedron possessing six equal bond lengths is unstable in terms of energy, and distortions with different bond lengths can lift the degeneracy, and thus reducing the energy. While in a strongly correlated electron system, it will cause a cooperative structural phase transition, namely, cooperative Jahn–Teller distortion or orbital ordering. The removal of orbital degeneracy in lattice is often accompanied by a reduction of lattice symmetry. By using the high spatial resolution TEM, we find that the Cr–O bond length along the *a*, *b*, and *c* axis is different. It is concluded that the ambient pressure and temperature phase of $SrCrO_3$ possess bonding instability, which leads the bond length to fluctuate, thereby explaining why the $SrCrO_3$ exhibits anomalous electronic states and transport properties. The calculated results of $SrCrO_3$ are in good agreement with our experimental observations, and the phonon band structure without any imaginary frequency suggests that our determined structure of $SrCrO_3$ is dynamically stable (Fig. S6 in the supplementary material).

IV. CONCLUSIONS

By using the TEM technique combined with first-principles calculations, we have carried out the structural analyses of perovskite chromate $SrCrO_3$ that contains unusual high-oxidation state Cr^{4+}. The SAED patterns suggest that $SrCrO_3$ does not possess cubic symmetry, and the EELS spectra along the three main directions exhibit that they are different from each other. The GGA+U calculation of the ELNES of the O-K edge is performed and the calculated results are in agreement with the experimental results. It is deduced that $SrCrO_3$ is not of cubic symmetry but possesses an orthorhombic structure. The lowering in crystal symmetry accords with Jahn-Teller theorem, indicating the bonding instability of $SrCrO_3$ at ambient pressure.[11] The EELS has been used as a sensitive probe for detecting the structure distortion and local electronic changes for decades, demonstrating that it is an effective technique.

SUPPLEMENTARY MATERIAL

The supplementary material presents the comparison between the simulated and measured electron diffraction patterns; the comparison of calculated total and projected DOS between the cubic structure and the orthorhombic structure; how the U_{eff} value affects the simulated EELS and DOS; calculated individual O EELS spectra for the three main zone directions; and the phonon dispersion relations of the orthorhombic $SrCrO_3$ (Pmmm).

ACKNOWLEDGMENTS

This work was supported by the National Key Research Program of China (Grant Nos. 2017YFA0206200, 2016YFA0300701, and 2018YFA0208402) and the National Natural Science Foundation of China (NNSFC) (Grant Nos. 11574376, 11874413, 11934017, and 51972333). One of the authors, X. Shen, was sponsored by the Youth Innovation Promotion Association of Chinese Academy of Sciences (No. 2019009). The numerical calculations were carried out at the Center for Quantum Simulation Sciences in the Institute of Physics, Chinese Academy of Sciences.

REFERENCES

[1]H. Fu and R. E. Cohen, Nature **403**, 281 (2000).
[2]R. E. Cohen, Nature **358**, 136 (1992).
[3]P. Grünberg, R. Schreiber, Y. Pang, M. B. Brodsky, and H. Sowers, Phys. Rev. Lett. **57**, 2442 (1986).
[4]R. Zhang, G. Read, F. Lang, T. Lancaster, S. J. Blundell, and M. A. Hayward, Inorg. Chem. **55**, 3169 (2016).
[5]A. C. Komarek, S. V. Streltsov, M. Isobe, T. Möller, M. Hoelzel, A. Senyshyn, D. Trots, M. T. Fernández-Díaz, T. Hansen, H. Gotou, T. Yagi, Y. Ueda, V. I. Anisimov, M. Grüninger, D. I. Khomskii, and M. Braden, Phys. Rev. Lett. **101**, 167204 (2008).
[6]P. A. Bhobe, A. Chainani, M. Taguchi, R. Eguchi, M. Matsunami, T. Ohtsuki, K. Ishizaka, M. Okawa, M. Oura, Y. Senba, H. Ohashi, M. Isobe, Y. Ueda, and S. Shin, Phys. Rev. B **83**, 165132 (2011).
[7]W. Xiao, D. Tan, X. Xiong, J. Liu, and J. Xu, Proc. Natl. Sci. U.S.A. **107**, 14026 (2010).
[8]Á. M. Arévalo-López and M. Á. Alario-Franco, J. Solid State Chem. **180**, 3271 (2007).
[9]B. L. Chamberland, Solid State Commun. **5**, 663 (1967).
[10]A. J. Williams, A. Gillies, J. P. Attfield, G. Heymann, H. Huppertz, M. J. Martínez-Lope, and J. A. Alonso, Phys. Rev. B **73**, 104409 (2006).
[11]J. S. Zhou, C. Q. Jin, Y. W. Long, L. X. Yang, and J. B. Goodenough, Phys. Rev. Lett. **96**, 046408 (2006).
[12]L. Ortega-San-Martin, A. J. Williams, J. Rodgers, J. P. Attfield, G. Heymann, and H. Huppertz, Phys. Rev. Lett. **99**, 255701 (2007).
[13]E. Castillo-Martínez and M. Á. Alario-Franco, Solid State Sci. **9**, 564 (2007).
[14]A. M. Arévalo-López, E. Castillo-Martínez, and M. Á. Alario-Franco, J. Phys. Condens. Matter **20**, 505207 (2008).
[15]K.-W. Lee and W. E. Pickett, Phys. Rev. B **80**, 125133 (2009).
[16]Y. Qian, G. Wang, Z. Li, C. Jin, and Z. Fang, New J. Phys. **13**, 053002 (2011).
[17]M. Verma, B. Geisler, and R. Pentcheva, Phys. Rev. B **100**, 165126 (2019).
[18]K. H. L. Zhang, P. V. Sushko, R. Colby, Y. Du, M. E. Bowden, and S. A. Chambers, Nat. Commun. **5**, 4669 (2014).

[19]M. Bugnet, G. Radtke, and G. A. Botton, Phys. Rev. B **88**, 201107(R) (2013).
[20]L. P. Cao, L. Q. Pan, W. M. Li, X. C. Wang, Q. Q. Liu, Y. W. Long, C. Z. Gu, and C. Q. Jin, Int. J. Mod. Phys. B **29**, 1542025 (2015).
[21]P. Blaha, K. Schwarz, G. K. H. Madsen, D. Kvasnicka, and J. Luitz, *WIEN2 K, An Augmented Plane Wave + Local Orbitals Program for Calculating Crystal Properties* (Karlheinz Schwarz, Techn. Universität Wien, Austria, 2001), ISBN: 3-9501031-1-2.
[22]J. P. Perdew, K. Burke, and M. Ernzerhof, Phys. Rev. Lett. **77**, 3865 (1996).
[23]R. F. Egerton, *Electron Energy Loss Spectroscopy in the Electron Microscope*, 2nd ed. (Plenum Press, New York, 1986).
[24]K. Momma and F. Izumi, J. Appl. Crystallogr. **44**, 1272 (2011).
[25]S. P. Gao, C. J. Pickard, M. C. Payne, J. Zhu, and J. Yuan, Phys. Rev. B **77**, 115122 (2008).
[26]S. P. Gao, C. J. Pickard, A. Perlov, and V. Milman, J. Phys. Condens. Matter **21**, 104203 (2009).
[27]D. I. Khomskii, *Transition Metal Compounds* (Cambridge University Press, 2014).